Impact of magnetic fields on anisotropy in $Ca_3Ru_2O_7$

S. McCall,[1] G. Cao,[2] and J. E. Crow[1]
[1]*National High Magnetic Field Laboratory, Florida State University, Tallahassee, Florida 32310*
[2]*Department of Physics and Astronomy, University of Kentucky, Lexington, Kentucky 40506*
(Received 7 August 2001; revised manuscript received 9 January 2003; published 31 March 2003)

$Ca_3Ru_2O_7$ is a bilayered metallic paramagnet that orders antiferromagnetically at $T_N = 56$ K while remaining metallic and then undergoes a spin reorientation coincident with a metal-nonmetal transition at $T_M = 48$ K, entering a metamagnetic state. Low-temperature specific-heat measurements in magnetic fields show that the electronic specific heat, $\gamma = 44$ mJ/mol K^2, is field independent above and below the 6-T critical field, whereas the first-order nature of the metamagnetic transition is reflected by a small shift in the Debye temperature. Magnetization, electrical resistivity, and specific-heat measurements were performed on high-quality single crystals, allowing construction of detailed *H-T* phase diagrams, which differ considerably for magnetic fields applied along the two in-plane directions. These measurements led to determination of the anisotropy field $H_A = 22.4$ T and exchange field $H_E = 14.2$ T. Evidence is presented for a possible flopside state in the region above the 41-K and 5.5-T multicritical point. Finally, superheating and supercooling are observed at temperatures and magnetic fields slightly above the multicritical point.

DOI: 10.1103/PhysRevB.67.094427 PACS number(s): 75.30.Gw, 71.30.+h, 75.30.Kz, 65.40.Gr

I. INTRODUCTION

The Ruddlesden-Popper series of ruthenates, with the general form $(Sr, Ca)_{n+1}Ru_nO_{3n+1}$, are perovskite-like systems consisting of n layers of corner-sharing RuO_6 octahedra separated by a rocksalt layer (SrO or CaO). Collectively, they exhibit a wide variety of magnetic phenomena including superconductivity,[1] metal-insulator transitions,[2,3] itinerant ferromagnetism,[4] and metamagnetism.[2] One particularly interesting aspect is that while Ca and Sr are isovalent, the analogous systems are remarkably divergent, as dramatically illustrated by the single-layered $(Ca, Sr)_2RuO_4$ members in which the Sr_2RuO_4 becomes superconducting[5] with $T_c = 1.5$ K while the equivalent Ca analog has an insulating antiferromagnetic ground state with the resistivity rising a remarkable nine orders of magnitude[3] between room temperature and 77 K. In a similar albeit less dramatic fashion, the infinite-layered $SrRuO_3$ system is metallic and orders ferromagnetically at 165 K, while metallic $CaRuO_3$ does not order at all (for $T > 30$ mK) (Ref. 6) yet a paramagnetic Weiss temperature (-8 K) suggests antiferromagnetic correlations.[7] Since the formal valances of the Ca and Sr are identical, the critical factor determining these vastly different properties must predominantly arise from distortions to the crystal structure resulting from substitution of Sr^{+2} ($r_{Sr} = 1.18$ Å) by the considerably smaller Ca^{+2} ($r_{Ca} = 1.00$ Å).

These distortions lead to differing Ru-O-Ru bond angles which in turn regulate the electronic bandwidth W. The ratio between W and U, the on-site Coulomb repulsion, controls the electrical transport properties.[8] This effect is elegantly illustrated by comparing the single-layered Ruddlesden-Popper ruthenates mentioned above. Sr_2RuO_4, which has Ru-O-Ru bond angles of 180°, forms an ideal tetragonal system,[9] while the distorted orthorhombic Ca_2RuO_4 ($a = 5.4022$, $b = 5.4932$ Å) has Ru-O-Ru bond angles of 151° in the planes and RuO_6 octahedra that tilt about 9.3° away from the c axis.[10] Similarly, two-layered $Sr_3Ru_2O_7$ remains essentially tetragonal although the octahedra twist within the plane[11,12] so that the intraplanar Ru-O-Ru bond angle is approximately 166°, but does not tilt away from the c axis, thus the interplanar Ru-O-Ru bond angle is 180°. On the other hand, $Ca_3Ru_2O_7$, the subject of this paper, has both twisting (intraplane bond angles: 149.87°–150.47°) and tilting (interplane angle: 152.13°) RuO_6 octahedra.

Initially, $Ca_3Ru_2O_7$ was reported as possessing a tetragonal structure,[2] but later single-crystal x-ray-diffraction studies showed that it belongs to the orthorhombic space group $Bb2_1m$ (the standard setting is $Cmc2_1$, but by using $Bb2_1m$ the c axis may be defined as perpendicular to the metal oxide planes, consistent with the vast literature on layered transition-metal-oxide systems) with lattice constants[13] at 173 K of $a = 5.3720(6)$, $b = 5.5305(6)$, and $c = 19.572(2)$ Å where the difference between the a and b lengths arise predominantly due to the interplanar tilt between neighboring RuO_6 octahedra. This tilt projects primarily onto the ac plane (153.22°) while only slightly impacting the bc plane (172.0°), the details of which are described elsewhere.[13] Furthermore, this appears to be the crucial bond angle defining the physical properties within the system, as will be shown by developing two very different magnetic phase diagrams for H applied along a and b, respectively. This is particularly interesting because it clearly demonstrates the impact of structural distortions on the physical properties; furthermore it permits investigation of the interaction between the spins and lattice distortions within not only the same material, but also the same sample merely by rotating the magnetic field 90°. By contrast, the intraplane Ru-O-Ru bonds lie along the [110] direction—consistent with the habit of these crystals to grow as plates with the in-plane principal crystallographic axes along the diagonals of the crystal, rather than along the edges.

Previous work[2,13,14] examined some properties of this system in a magnetic field, but this is the first time measurements of the properties in a magnetic field along the two

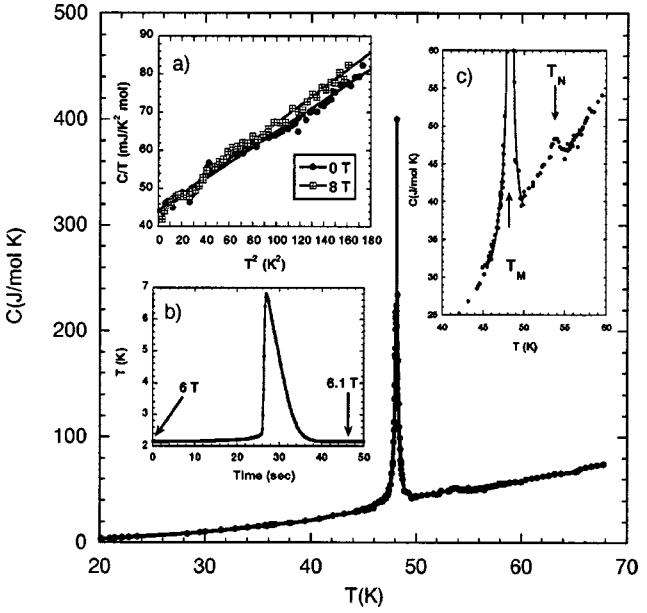

FIG. 1. Specific heat versus temperature showing a large peak at T_M ($=48$ K). (a) C/T vs T^2 for 0 and 8 T, showing electronic and phononic contributions. (b) ''Adiabatic'' measurement of temperature as B is swept at ~ 25 G/s, demonstrating spontaneous heating at the metamagnetic transition. (c) Enlargement of high-temperature region, showing a minuscule peak at the Néel temperature.

in-plane directions have been reported for high-quality untwinned single crystals, and we report on properties with the magnetic field applied along the b axis. These high-quality and untwinned crystals were grown using a self-flux approach, and confirmed by Laue diffraction, which also permits the unambiguous assignment of the metamagnetic axis along the a axis [5.3720(6) Å].

II. SPECIFIC-HEAT MEASUREMENTS

The low-temperature specific heat was measured using a quasiadiabatic heat pulse method[15] on an 8.32-mg parquet of carefully aligned single crystals ($\mathbf{H}\|a$). The results over the range $2<T<13$ K at $H=0$ and 8 T are plotted as C/T vs T^2 in Fig. 1(a) where a linear fit to the data results in a Debye temperature of $\theta_D=480$ K (465 K) for a magnetic field of 0 T (8 T), similar to comparable two-layer metal-oxide systems.[16] The shift in θ_D by 15 K in 8 T may reflect the first-order transition that occurs when crossing the $H_c=6$ T phase boundary. The linear term, on the other hand, remains constant at $\gamma=44\pm 2$ mJ/mol K^2, and indicates either highly correlated electrons or partially localized states near the Fermi surface. This is comparable with the metallic members of the Ruddlesden-Popper ruthenate series,[7,17,18] which vary from 30 to 110 mJ/mol-Ru K^2, even though the resistivity for $Ca_3Ru_2O_7$ suggests that the system is nonmetallic ($d\rho/dT<0$) in this temperature range. Despite the dramatic change in the resistivity and magnetization[2] observed for $\mathbf{H}(\|a)>6$ T, the electronic contribution to the specific heat remains constant, indicating no significant change in the electronic density of states (DOS) above the metamagnetic transition. In a two-layered system such as $Ca_3Ru_2O_7$, this suggests a type-A antiferromagnetic structure—ferromagnetically aligned planes coupled together antiferromagnetically—since flipping neighboring planes from antiferromagnetic to ferromagnetic alignment does not change the size of the magnetic Bravais lattice. Conversely, were the Ru moments aligned antiferromagnetically within the individual planes, flipping neighboring spins would double the size of the Brillioun zone which ought to be reflected by a significant change in the electronic DOS at the Fermi surface. Therefore, the dramatic drop in resistivity that occurs at the metamagnetic transition must relate more closely to a change in the carrier mobility, driven by a possible sudden reduction in spin scattering as the spins flip from antiferromagnetic to ferromagnetic alignment.

For a three-dimensional (3D) system, ferromagnetic and antiferromagnetic spin-wave contributions to the specific heat are proportional to $T^{3/2}$ and T^3, respectively. Attempts to include a $T^{3/2}$ term in the specific heat did not improve the fit, further arguing against the presence of 3D magnons, and the T^3 term, increases slightly at 8 T, ruling out 3D antiferromagnetic spin waves, since destruction of the antiferromagnetic ordering (>6 T) would decrease the T^3 contribution were they present at 0 T. These results agree with the magnetic-susceptibility measurements, which are temperature independent for $T<30$ K, and thus show no evidence of spin waves at low temperatures. This outcome is expected for an Ising-like system, where an anisotropy gap on the order of $(g\mu_B k_B)\sqrt{2H_E H_A+H_A^2}\approx 45$ K for antiferromagnetic spin waves, and an even larger gap for ferromagnetic spin waves, rules out their appearance for temperatures much smaller than those at the gap.[19]

While the electronic specific heat remains nearly unchanged for magnetic fields above and below the metamagnetic transition, the transition itself is first order, so a latent heat may be observable. Figure 1(b) shows the temperature as a function of time for a 3.8-mg sample mounted on a quasiadiabatic calorimeter such that the applied field $\mathbf{H}\|a$ while the magnetic field is swept through the metamagnetic transition. At the metamagnetic transition, the sample temperature spontaneously jumps nearly 5 K, and then gradually decays back to its base temperature as the heat flows to the thermal bath, which is coupled to the sample by weak thermal links. A similar transition, equal in magnitude, occurs at about 5.1 T (at 2 K) when sweeping the magnetic field towards zero, consistent with the hysteresis loop observed in magnetization measurements. This phase transition is isentropic with respect to the spins, and releases latent heat as the magnetic field is swept in both directions; thus it is distinct from the magnetocaloric effect. The latent heat released at each transition was $L=8.4\pm 0.2$ J/mol at 2 K, leading to a total-energy release of $2L=16.8\pm 0.3$ J/mol released by sweeping the magnetic field up and down through the transition. This value compares exceptionally well to the hysteresis loss[20] of 17 J/mol at 2 K, obtained from $\oint M dH$. As expected, no comparable effect was observed when the sample was rotated so that $H\|b$.

The specific heat through the $T_M=48$ K spin-reorientation/metal-nonmetal transition and 56 K Néel temperature is shown in Fig. 1, with a large peak in $C(T)$ at T_M.

This peak is narrow and highly symmetric, consistent with other parameters, suggesting that the transition is first order and similar to spin-reorientation transitions observed in other systems,[21] such as $Dy_{0.25}Er_{0.75}Al_2$. In most metamagnetic systems, the zero-field transition is second order for temperatures above the critical point, which for $Ca_3Ru_2O_7$ occurs at 41 K and 5.5 T, as discussed in the next section; however, this assumes a transition from a paramagnetic to antiferromagnetic state. In the case of $Ca_3Ru_2O_7$, for small H, the transition is between two different antiferromagnetic states. The entropy removed under the peak, $\Delta S = 2.7 \pm 0.15$ J/mol K, is much smaller than $R \ln(3) = 9.125$ J/mol-Ru K (18.25 J/mol K) expected for an $\mathbf{S}=1$ system. However, that is an upper limit on spin entropy, assuming a transition from entirely random spins to a completely ordered spin system—clearly not the case, since above T_M the system is already antiferromagnetically ordered—thus the spin entropy available at 48 K should be well below this limit. Figure 1(c) shows an enlargement of the 40–60-K region, revealing an extremely small peak at 54 K near T_N. The entropy removed after subtracting a simple phonon and electron fit above 56 K yields an entropy change between 50 and 56 K of only ~0.3 J/mol K, which is an almost negligible fraction (~2%) of the potential $2R \ln(3)$ entropy change. The miniscule peak at the ordering temperature serves as an indication of possible itinerant magnetism, along with the noninteger saturation moment and large electronic contribution to the specific heat.

III. GENERAL MAGNETIC PROPERTIES

The magnetic susceptibility $\chi(T)$ is shown in the inset of Fig. 2(a) for **H** applied along all three principal crystal directions. At 56 K, there is a peak in χ_b ($\chi \| b$), while χ_a and χ_c become flat as a function of decreasing temperature for $56 \geqslant T \geqslant 48$ K, providing a nearly textbook example of antiferromagnetic ordering with the spins oriented along b. The second feature of note occurs at 48 K—a subtle change in slope of χ_b, contrasting with a sharp drop in χ_a and χ_c, which for the lowest temperatures leads to $\chi_a = 2$ emu/mol, while $\chi_b = \chi_c = 38$ emu/mol. Such behavior strongly implies a spin-reorientation transition to a new antiferromagnetic state with the spins spontaneously flopping from b to align along a. For $T < 35$ K, the magnetic susceptibility becomes temperature independent, indicating the absence of thermally excited spin waves, consistent with the Ising-like behavior expected of a metamagnetic system.[22]

The high-temperature magnetic susceptibility has been reported elsewhere,[2,20] and obeys the modified Curie-Weiss law with $\mu_{\text{eff}} = 2.86 \pm 0.08 \mu_B$/Ru in agreement with the $2.83 \mu_B$/Ru expected for Ru^{4+} in its low-spin ($S=1$) state. However, the Weiss temperature was determined to be +72, +59, and +64 K along the a, b, and c axes, respectively, which possess the wrong sign for an antiferromagnet. A positive Weiss (Curie) temperature indicates that ferromagnetic correlations dominate the magnetic interactions at high temperatures, suggesting that $Ca_3Ru_2O_7$ orders with type-A antiferromagnetism, that is, ferromagnetic planes coupled antiferromagnetically.[23–25] Competition between ferromagnetic and antiferromagnetic interactions is an essential characteristic common to metamagnetic systems.[22]

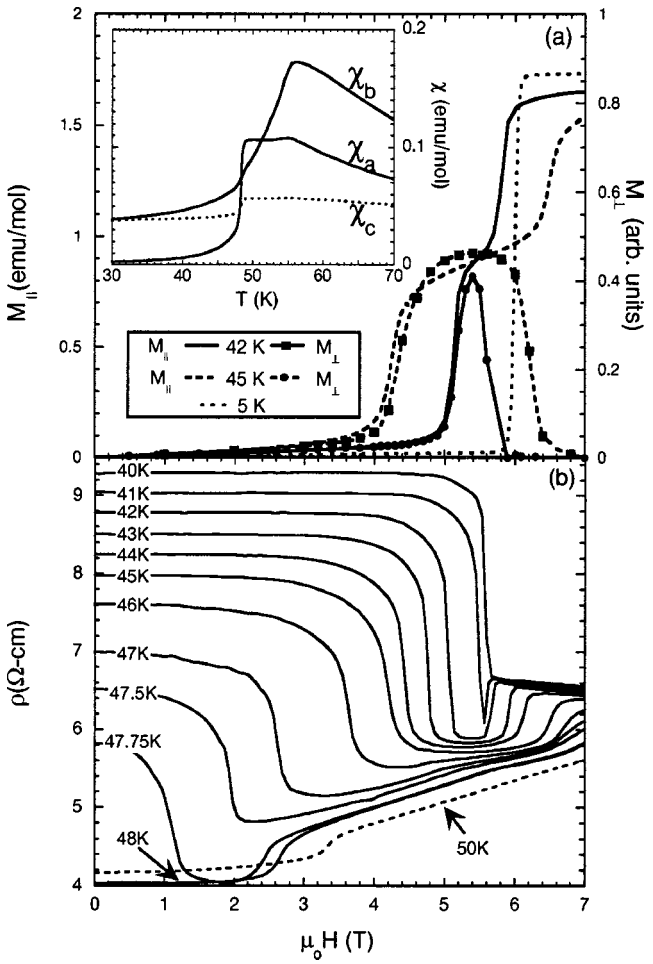

FIG. 2. Isothermal magnetization $\mathbf{M}_{\|}$ and isothermal transverse magnetization $M_\perp$, with $\mathbf{H} \| a$. The inset shows $\chi(T)$ for $\mathbf{H} \|$ to the $a-c$ axes, illustrating typical antiferromagnetic ordering at $T_N = 56$ K, and the spin-reorientation transition at $T_M = 48$ K. (b) Isothermal magnetoresistivity with $H \| a$.

In a typical antiferromagnet, using the molecular-field model, when the applied magnetic field along the spin direction exceeds a critical value given by $H_{\text{SF}} = (2H_E H_A - H_A^2)^{1/2}$, the system undergoes a spin-flop transition, characterized by a jump in the magnetization, where H_E is the exchange field and normally greatly exceeds H_A, the anisotropy field. Above the spin-flop transition, the magnetization gradually increases until it saturates at the critical field:[19,26]

$$H_c(T=0) = 2H_E - H_A. \tag{1}$$

However, metamagnetic systems by definition[22,26] have an $H_A > H_E$, so there is no stable spin-flop state, rather the spins flip immediately to a saturated state at the critical field of Eq. (1) above. Combining this equation with[19,26]

$$\chi_\perp(T=0) = \frac{M_S}{2H_E + H_A} \tag{2}$$

permits calculation of H_E and H_A using H_c (6 T), $\chi_\perp$ (3.8×10^{-2} emu/mol), and the saturation magnetization ($M_S = 1.73\mu_B$/Ru). Solving these equations results in values of $H_E = 14.2$ and $H_A = 22.4$ T, confirming $H_A > H_E$ and consistent with critical values determined via resistivity and heat-capacity measurements as discussed in appropriate sections.

IV. PROPERTIES WITH H∥*a*

As previously reported,[2] a metamagnetic transition, where the moment changes from nearly 0 to $1.73\mu_B$/Ru (close to the $2\mu_B$/Ru expected for the $S=1$ state), occurs when $\mathbf{H}\|a$ at a critical magnetic field of 6 T with increasing field and 5.3 T for decreasing field at $T=5$ K. The 0.7-T wide hysteresis loop proves the transition is first order with respect to **H**. By contrast when $\mathbf{H}\|b$, $\mathbf{M}(\mathbf{H})$ is linear, presenting neither a corresponding feature at 6 T nor any evidence of hysteresis. The field-independent value of M when $H(\|a) > 6$ T indicates the system is saturated, which is further supported by pulsed field magnetization data to 60 T, showing no additional field-induced transitions.[27]

At low temperatures the easy axis is along *a*, while above the spin-reorientation transition T_M the easy axis is along *b*. Application of $H\|a$ depresses T_M toward a multicritical point[2] (MCP) near 41 K and 5.5 T, and leads to additional magnetic phases. This section explores the impact of $H\|a$ on the phase boundaries through careful measurement of magnetoresistivity, magnetization, and heat capacity. The results of these measurements, summarized in Fig. 2, then permit construction of an HT phase diagram for $Ca_3Ru_2O_7$.

Isothermal longitudinal magnetization, i.e., $M\|H$, measurements presented in Fig. 2(a) include a 5-K trace illustrating the metamagnetic transition observed for $T<41$ K, while for the two higher-temperature traces (42 and 45 K), the metamagnetic transition splits into two distinct steps of equal magnitude, so that above the initial step, the magnetization is approximately one-half the saturation moment. The separation between the steps increases with temperature until the spin-reorientation temperature (48 K), where they disappear. The transverse magnetization $M_\perp$, which measures the moment perpendicular to the external applied magnetic field, i.e., $H\|a$, $M\perp H$, is also shown in Fig. 2(a). The transverse magnetization $M_\perp$ is large when the longitudinal moment is $\sim\frac{1}{2}M_{\rm sat}$ and negligible elsewhere. Together, these results imply that the system undergoes a flopside transition to a state where half the planes are aligned ferromagnetically (FM)$\|a$ and half are FM$\|b$ with a magnetic spin structure similar to HoP.[28]

Measurement of the isothermal magnetoresistivity as shown in Fig. 2(b) for temperatures $40 \leqslant T \leqslant 50$ K provides an additional probe of the magnetic phase diagram. Note that when the temperature is below the MCP, there is a single magnetic phase boundary at the critical magnetic field, identifiable by a sharp drop in the magnetoresistivity, and indicating a change from antiferromagnetic-nonmetallic (AFNM) to ferromagnetic-nonmetallic FNM order, with spins oriented along *a* in both phases as illustrated by the 40 K trace. At 41 K, the sharp drop remains, but there is an almost immediate jump afterwards, marking the MCP as a magnetoresistive minimum. As the temperature increases, these two features—the drop and the jump—separate, moving to lower and higher magnetic fields respectively, with the drop disappearing at 48 K, while the jump broadens considerably. The region of minimal isothermal magnetoresistivity mirrors the plateau in the isothermal magnetization, where the drop tracks the first step in $M(H)$ and the jump tracks the second, which is evident when comparing Figs. 2(a) and 2(b). The lower magnetoresistivity in this intermediate region as compared to the AFNM and FNM regions supports the argument for a flopside transition: the resistivity is lowest when the spins are aligned along *b*, so a state with half the spins aligned along *b* ought to have a resistivity between the antiferromagnetic-metallic-*b* (AFM-*b*) and FNM (spins along *a*) phases.

At temperatures just below 48 K a new kink arises at $\sim$2.5 T, which increases in magnetic field with temperature to a maximum of 3.5 T at 52 K and then decreases to zero by T_N, an example of which is illustrated by the 50 K trace in Fig. 2(b). In small magnetic fields, the 48 K trace has a smaller resistivity than the 50-K trace, altering the trend of resistivity decreasing as temperature increases, and illustrating that the system is metallic ($d\rho/dT>0$) above 48 K for small *H*. At the kink in the 48-K trace, it crosses the 50-K trace so that $d\rho/dT<0$, suggesting that this kink corresponds to the destruction of the metallic state (AFM-*b*). Overall, the features in the isothermal magnetoresistivity offer some insight into the phase diagram, where the drop in $\rho(H)$ indicates the destruction of the AFNM state; the jump in $\rho(H)$ indicates the FNM transition; the upturn arising at low *H* only at higher temperatures (47.75–50 K) indicates the antiferromagnetic-metallic boundary (AFM-*b*); and finally the flopside phase occupies the region between the drop and jump in the isothermal $\rho(H)$. This leads directly to construction of a more complete phase diagram for $H\|a$, shown in Fig. 3. However, microscopic probes, in the $40<T<50$ K and $0<H<8$ T range, such as neutron scattering are needed to clarify the magnetic structure, especially in the proposed ferrimagnetic (shaded) region of Fig. 3(a). Simple diagrams of the proposed spin structures for the ordered phases are shown in Fig. 3(b).

The peak in the specific heat at T_M in zero magnetic field shrinks in magnitude and broadens considerably as $H\|a$ increases (data not shown). The peak also shifts to lower temperatures as *H* increases, and the entropy removed under the peak projects to zero between 5 and 5.5 T, i.e., near the MCP. However, at magnetic fields and temperatures just above the MCP, superheating and supercooling effects are observed, and a new specific-heat anomaly arises. Such effects are only observed in exceptionally pure samples, thus confirming the very high quality of these crystals. Figure 4 shows the temperature of a sample as a function of time as heat is applied (removed) in a magnetic field of 6 T. At the critical temperature, the sample spontaneously cools (warms) by 0.51 K (0.66 K). A likely explanation for such behavior is that the spins disorder (order) as the critical temperature is approached from below (above), and that they spontaneously absorb (release) entropy as they change states. Thermal lattice vibrations are the most readily available entropy source

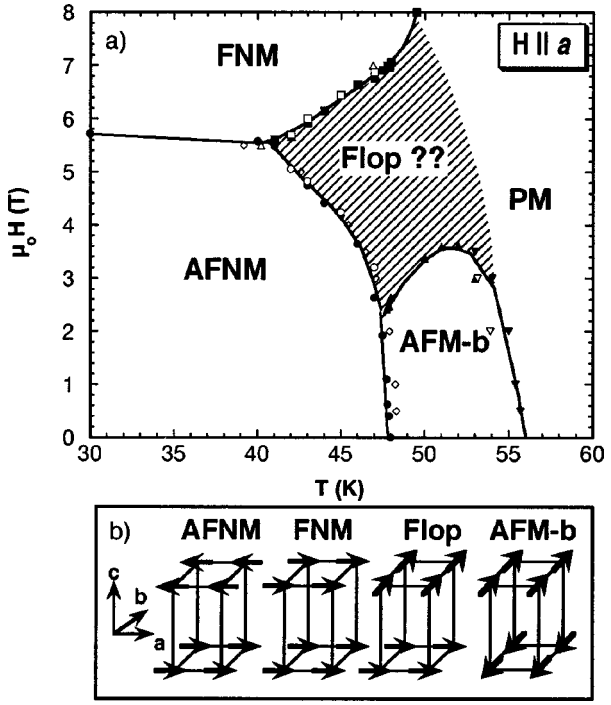

FIG. 3. (a) Phase diagram for *HT* plane with $H \| a$. The regions are antiferromagnetic nonmetal (AFNM), ferromagnetic nonmetal (FNM), antiferromagnetic metal (AFM-b), paramagnetic metal (PM), and a complex region that may include a ferrimagnetic flop-side type of magnetic structure. Data points were obtained from isothermal magnetoresistivity and constant *H* resistivity (solid shapes), and magnetization (open shapes). (b) Simple models illustrate each ordered phase with the crystallographic axes defined along the left edge.

(sink), with the result that this phase change is reflected by a change in the sample temperature via superthermal effects. From the anomalous portion of the curve, the entropy change due to this superthermal effect is 0.69 ± 0.03 for the warming case and 0.99 ± 0.03 J/mol K for cooling, assuming that all of the crystals in the sample experience this effect. The inset of Fig. 4 shows the heat capacity in the vicinity of these superthermal effects, where there is a thermal hysteresis—a peak is observed when T_c is approached from below, but no such feature is observed when cooling through this same temperature range. Integrating the difference between the two curves results in an entropy change of $\Delta S = 0.28 \pm 0.04$ J/mol K, in agreement with the entropy difference between the two superthermal effects (i.e., $0.99 - 0.69 = 0.30$ J/mol K). These effects, along with the spontaneous heating discussed in the specific-heat section, lead to the conclusion that the phase boundary defining the field-induced ferromagnetic state (FNM) is strongly first order and distinct from the saturated paramagnetic state expected for most simple metamagnets.

V. PROPERTIES WITH H||*b*

Application of magnetic fields along *b* leads to a significantly different phase diagram from that of Fig. 3. It is constructed in the following section by once again carefully examining the resistivity, magnetization, and specific heat in a

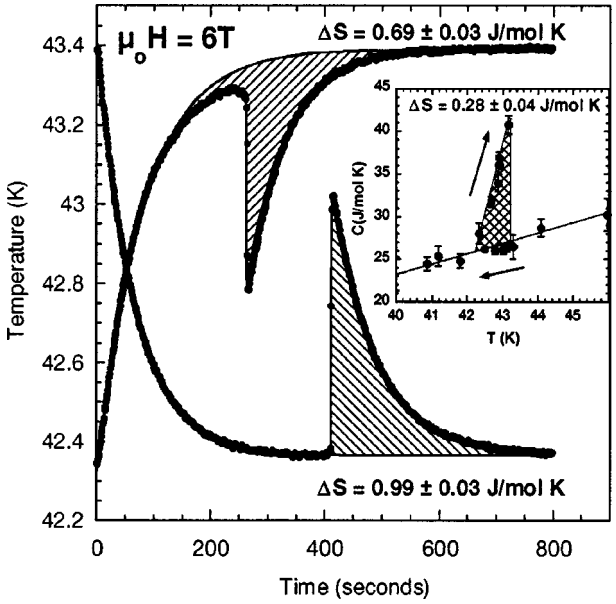

FIG. 4. Superheating and supercooling curves obtained in 6 T during quasiadiabatic heat pulse measurements. The hatched area was used to calculate the entropy change. Inset shows heat-capacity hysteresis between the onset of the superthermal curves—a peak is observed if the measurement is made by approaching from low temperatures, while no such peak is observed when cooling from higher temperatures.

series of magnetic fields as illustrated in Fig. 5. Small magnetic fields along *b* suppress T_N, illustrated in the inset of Fig. 5(a) by the shift of the Fisher-Langer anomaly in the resistivity as the magnetic field increases. A corresponding peak is observed in dM/dT as a function of temperature for similar magnetic fields (not shown). This shift in the onset temperature of the AFM-*b* state is rapid so that by 3 T it disappears with the transition moving from a paramagnetic state directly to the AFNM state. At magnetic fields less than 3 T, $T_M = 48$ K remains essentially constant, observable as the sharp resistivity upturn in the inset of Fig. 5(a). Larger magnetic fields gradually suppress T_M demonstrated in Fig. 5 by the jump in the resistivity, the drop in the magnetization, and the peak in the specific heat. The strong agreement between different measurements further demonstrates the close coupling between the spin and charge carriers within this system, while the heat-capacity measurement shows that application of a magnetic field along *b* suppresses the transition in both temperature and magnitude.

The data from Fig. 5 may be used to construct the *HT* phase diagram for $H \| b$ as shown in Fig. 6. This diagram is considerably less complex than that for $H \| a$, consisting only of AFM-*b*, AFNM, and paramagnetic (PM) phases, with a triple point arising at 48 K and 3 T. In magnetic fields above 5.5 T, the phase boundary between the PM and AFNM states fits very well to

$$H_M(T_M) = 22.4 - \frac{k_B T_M}{2gS\mu_B}, \tag{3}$$

where T_M is the critical temperature, H_M is the critical magnetic field, and the uncertainty in the intercept and slope

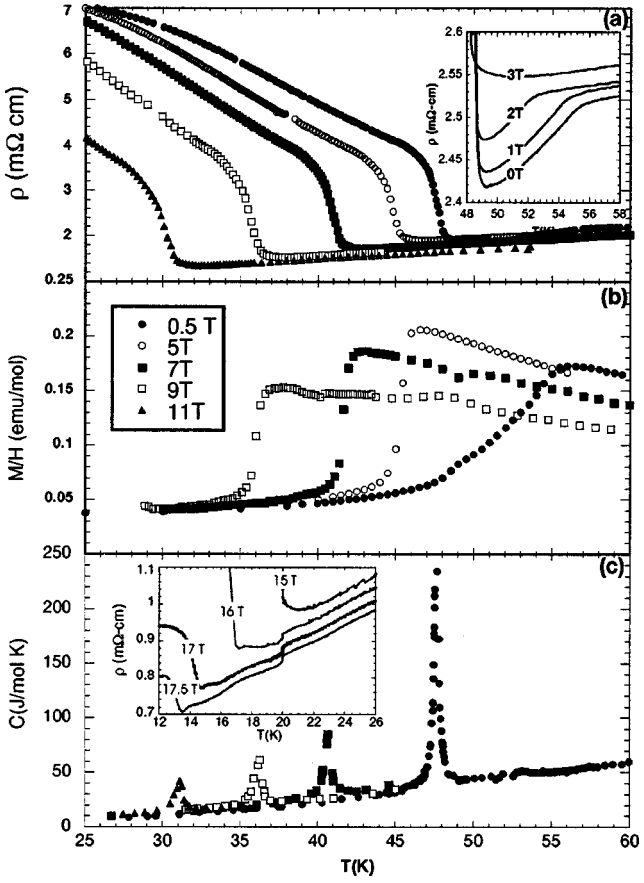

FIG. 5. (a) Resistivity, (b) magnetization, and (c) specific-heat data obtained for several values of $H\|b$. The inset of (a) shows the impact of magnetic fields $\leqslant 3$ T in suppressing the Néel temperature, while the inset of (c) shows the subtle change in ρ at 20 K for $\mu_0 H > 15$ T.

values are ± 0.1 T and ± 0.01 T/K, respectively. The zero-temperature intercept projects to $H_M(0\ \mathrm{K}) = 22.4$ T, in excellent agreement with the anisotropy field, $H_A = 22.4$ T determined from Eqs. (1) and (2). It is particularly interesting to note that by increasing $\mathbf{H}\|b$, both transitions to ordered states—the AFM and AFNM phases—are smoothly shifted down in temperature, permitting the resurgence of paramagnetism. By contrast, increasing **H** along *a* shifts T_N only slightly, and new ordered states arise as the field suppresses T_M.

The entropy removed at the transition as a function of magnetic field may be calculated from the area underneath the specific-heat peak, where examples for several fields are shown in Fig. 5(c). The entropy removed decreases linearly with increasing magnetic field for $6 < H < 12$ T as the inset of Fig. 6 shows, fitting $\Delta S = 2.68 - 0.178 \mu_o H$. In the limit of zero external field, $\Delta S = 2.68$ J/mol K, in excellent agreement with the entropy removed at 0 T, while projecting this line to $\Delta S = 0$ results in a magnetic field of 15 T, comparable to the exchange field $H_E (= 14.2\ \mathrm{T})$. When the applied external magnetic field exceeds the exchange field, the system has reached a saturated paramagnetic state,[26] thus there is no remaining spin entropy and $\Delta S_{\mathrm{spin}} = 0$, in agreement with the projection in the inset of Fig. 6.

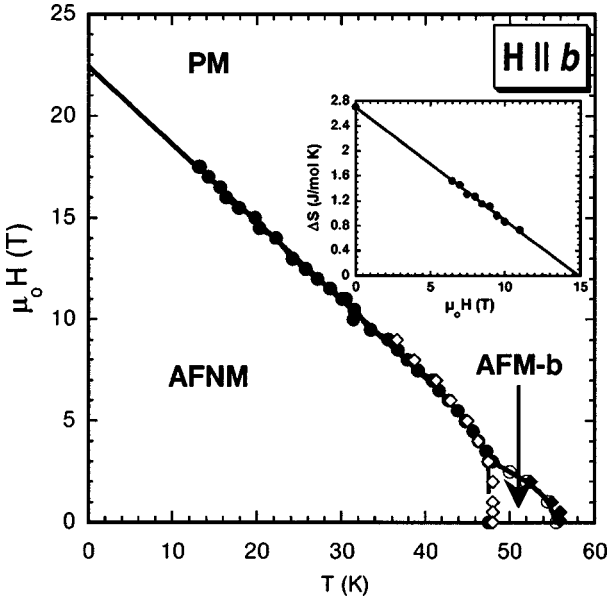

FIG. 6. The *HT* phase diagram for $H\|b$, defined by magnetization (open symbols) and resistivity (solid symbols) measurements. The inset shows entropy removed under the $T_M(H)$ peak with the line fit to the points between $6 < H < 12$ T, projecting to $\Delta S = 0$ at 15 T.

The inset of Fig. 5(c) shows the resistivity for several magnetic fields $15 \leqslant \mu_o H \leqslant 17.5$ T, illustrating two important features. The first is that $T_M(H)$, defining the AFNM boundary, continues to be depressed in temperature with increasing magnetic field to at least 17.5 T. This suggests that the entropy removed under the specific-heat peaks is distinct from the metal-to-nonmetal transition. The second feature is the small kink that occurs at 20 K in magnetic fields above 15 T. Energetically, $20\ \mathrm{K} \approx 14.9\ \mathrm{T} \approx H_E$, so this kink may reflect the loss of spin-dependent scattering contributions to the resistivity, arising from paramagnetic saturation as suggested by the discussion of entropy above.

VI. SUMMARY

Measurement of high-quality single-crystal samples of $Ca_3Ru_2O_7$ with magnetic fields applied parallel to both of the in-plane principal crystal axes results in two very distinct *HT* phase diagrams. This demonstrates a remarkable anisotropy in this system as compared to tetragonal $Sr_3Ru_2O_7$, resulting from smaller Ca ions replacing Sr, thus orthorhombically distorting the structure, and leading to a very rich phase space. The orthorhombic distortion may be almost completely accounted for by an examination of the tilting between RuO_6 octahedra in adjacent planes, where the tilt is much greater along *a* than *b*. The anisotropy is most clearly illustrated by the appearance of a metamagnetic state at low temperatures where the spins become locked along *a*, which might result from a structural transition at $T_M = 48$ K. Measurements of magnetization indicate the anisotropy field is $H_A = 22.4 \pm 0.4$ T, and that the exchange field is $H_E = 14.2 \pm 1$ T. These values are also reflected in specific-heat and resistivity measurements, arguing that the spin and charge

carriers are strongly coupled, and that the spin interactions are key to understanding the overall properties of this system.

At low temperatures, the large electronic contribution to the specific heat $\gamma = 44 \pm 2$ mJ/mol K^2 indicates a significant electronic DOS at the Fermi surface, despite nonmetallic behavior; thus the electrons must be highly correlated. Furthermore, this value is constant both above and below the 6-T critical field, indicating that the Fermi surface is largely unperturbed by the metamagnetic transition, supporting speculation that the system orders as a type-A antiferromagnet, since spin flips would leave the size of the magnetic Bravais lattice unchanged. Crossing H_c at low temperatures spontaneously heats the sample, while superthermal effects are observed in large magnetic fields above the multicritical point, distinctly segregating the ferromagnetic region (FNM) from the rest of the phase diagram by strong first-order transitions. Measurements in the temperature region just above the multicritical point with $\mathbf{H} \| a$ suggest a flopside phase similar to *HoP*, making this an ideal candidate for additional work with a microscopic probe such as neutron scattering or magnetic x-ray scattering.

ACKNOWLEDGMENTS

The authors would like to thank R. P. Guertin, C. S. Alexander, and A. D. Bianchi for useful discussions and a careful reading of this manuscript. This work was supported by NSF Grant No. DMR00-84173 and the State of Florida.

[1] Y. Maeno, H. Hashimoto, K. Yoshida, S. Nishizaki, T. Fujita, J. G. Bednorz, and F. Lichtenberg, Nature (London) **372**, 532 (1994).
[2] G. Cao, S. McCall, J. E. Crow, and R. P. Guertin, Phys. Rev. Lett. **78**, 1751 (1997).
[3] C. S. Alexander, G. Cao, V. Dobrosavljevic, S. McCall, J. E. Crow, E. Lochner, and R. P. Guertin, Phys. Rev. B **60**, R8422 (1999).
[4] P. B. Allen, H. Berger, O. Chauver, L. Forro, T. Jarlborg, A. Junod, B. Revaz, and G. Santi, Phys. Rev. B **53**, 4393 (1996).
[5] Y. Maeno, Z. Q. Mao, S. Nishizaki, and T. Akima, Physica B **280**, 285 (2000).
[6] M. M. Shepard, Ph.D. dissertation, Florida State University, 1998.
[7] G. Cao, S. McCall, M. Shepard, J. E. Crow, and R. P. Guertin, Phys. Rev. B **56**, 321 (1997).
[8] P. A. Cox, *Transition Metal Oxides* (Clarendon, Oxford, 1995).
[9] L. Walz and F. Lichtenberg, Acta Crystallogr., Sect. C: Cryst. Struct. Commun. **C49**, 1268 (1993).
[10] M. Braden, G. Andre, S. Nakatsuji, and Y. Maeno, Phys. Rev. B **58**, 847 (1998).
[11] Q. Huang, J. W. Lynn, R. W. Erwin, J. Jarupatrakorn, and R. J. Cava, Phys. Rev. B **58**, 8515 (1998).
[12] H. Shaked, J. D. Jorgensen, O. Chmaissem, S. Ikeda, and Y. Maeno, J. Solid State Chem. **154**, 361 (2000).
[13] G. Cao, K. Abboud, S. McCall, J. E. Crow, and R. P. Guertin, Phys. Rev. B **62**, 998 (2000).
[14] H. L. Liu, S. Yoon, S. L. Cooper, G. Cao, and J. E. Crow, Phys. Rev. B **60**, R6980 (1999).
[15] R. Bachmann, F. J. DiSalvo, Jr., T. H. Geballe, R. L. Greene, R. E. Howard, C. N. King, H. C. Kirsch, K. N. Lee, R. E. Schwall, H.-U. Thomas, and R. B. Zubeck, Rev. Sci. Instrum. **43**, 205 (1972).
[16] S. Ikeda, Y. Maeno, and T. Fujita, Phys. Rev. B **57**, 978 (1998).
[17] S. Ikeda, Y. Maeno, S. Nakatsuji, M. Kosaka, and Y. Uwatoko, Phys. Rev. B **62**, 6089 (2000).
[18] G. Cao, S. McCall, M. Shepard, J. E. Crow, and R. P. Guertin, Phys. Rev. B **56**, R2916 (1997).
[19] L. J. D. Jongh and A. R. Miedema, Adv. Phys. **50**, 947 (2001).
[20] S. McCall, Ph.D. thesis, Florida State University, 2000.
[21] A. M. Tishin, J. K. A. Gschneidner, and V. K. Pecharsky, Phys. Rev. B **59**, 503 (1999).
[22] E. Stryjewski and N. Giordano, Adv. Phys. **26**, 487 (1977).
[23] J. B. Goodenough, *Magnetism and the Chemical Bond* (Wiley, New York, 1963).
[24] M. Kubota, Y. Oohara, H. Yoshizawa, H. Fujioka, K. Shimizu, K. Hirota, Y. Moritomo, and Y. Endoh, J. Phys. Soc. Jpn. **69**, 1986 (2000).
[25] M. Kubota, H. Fujioka, K. Ohoyama, K. Hirota, Y. Moritomo, H. Yoshizawa, and Y. Endoh, J. Phys. Chem. Solids **60**, 1161 (1999).
[26] R. L. Carlin and A. J. v. Duyneveldt, in *Magnetic Properties of Transition Metal Compounds* (Springer-Verlag, New York, 1977).
[27] R. P. Guertin (private communication).
[28] T. O. Brun, G. H. Lander, F. W. Kobty, and J. S. Kouvel, in *Magnetism and Magnetic Materials—1974*, edited by C. D. Graham, Jr., G. H. Lander, and J. J. Rhyne, AIP Conf. Proc. No. 24 (AIP, New York, 1975), p. 244.